Research Article | Vol. 10, No. 11 / 1 November 2019 / Biomedical Optics Express 5703
Biomedical Optics EXPRESS

Methods of extraction of optical properties from diffuse reflectance measurements of ex-vivo human colon tissue using thin film silicon photodetector arrays

BEN LARIVIERE,[1,*] N. LYNN FERGUSON,[2] KATHERINE S. GARMAN,[3] DEBORAH A. FISHER,[3] AND NAN M. JOKERST[1]

[1]Department of Electrical and Computer Engineering, Duke University, Durham, NC 27708, USA
[2]Duke University Department of Pathology, Durham, NC 27710, USA
[3]Duke University Department of Medicine, Durham, NC 27710, USA
[*]benjamin.lariviere@duke.edu

Abstract: Spatially resolved diffuse reflectance spectroscopy (SRDRS) is a promising technique for characterization of colon tissue. Herein, two methods for extracting the reduced scattering and absorption coefficients ($\mu_s'(\lambda)$ and $\mu_a(\lambda)$) from SRDRS data using lookup tables of simulated diffuse reflectance are reported. Experimental measurements of liquid tissue phantoms performed with a custom multi-pixel silicon SRDRS sensor spanning the 450 - 750 nm wavelength range were used to evaluate the extraction methods, demonstrating that the combined use of spatial and spectral data reduces extraction error compared to use of spectral data alone. Additionally, SRDRS measurements of normal and tumor ex-vivo human colon tissue are presented along with $\mu_s'(\lambda)$ and $\mu_a(\lambda)$ extracted from these measurements.

1. Introduction

Inflammatory bowel diseases (IBD), Crohn's disease and ulcerative colitis, is associated with an increased risk of colorectal cancer. To detect cancer at an earlier and more treatable stage, colonoscopy surveillance is recommended for patients with IBD [1]. The present standard of care is to inspect the colonic lumen surface using white light endoscopy (WLE) and take random biopsies to detect dysplasia (abnormal cellular growth indicative of pre-cancer) and malignancy (cancer). While WLE is effective for the detection of some high-risk tissues such as colon polyps, other types of high-risk tissue, such as flat dysplasia, may not be visually observable to the physician by WLE [2,3]. The limited efficacy of WLE results in reduced adenoma detection rates, unnecessary resection of healthy tissues, incomplete resection of high-risk tissues, and necessitates random sampling of colon in patients known to be at elevated risk for flat dysplasia, such as patients with inflammatory bowel disease [2,3]. Patient outcomes for colon cancer can be improved if the capabilities of WLE can be augmented to readily detect the microstructural and biochemical characteristics of this disease during colonoscopy.

Diffuse reflectance spectroscopy (DRS) is a label free optical technique that has been established as an effective tool for optical characterization of human tissue, both by extraction of tissue optical properties [4–7], and by determining classifiers based on the spectral signatures of various tissues and conditions [8,9]. Measured DRS signals are sensitive to the concentrations of chromophores such as oxy-hemoglobin and deoxy-hemoglobin in tissue and can quantitatively measure these concentrations through measurement of the tissue absorption coefficient, $\mu_a(\lambda)$ [6,10]. Similarly, DRS is sensitive to tissue microstructure and morphology because the difference in the optical refractive index between tissue structures such as cellular nuclei and collagen fibers and the surrounding components of tissue causes tissue to scatter light in a manner that is characteristic of that tissue [11]. The wavelength dependent scattering characteristic of light in tissue can be

#374185 https://doi.org/10.1364/BOE.10.005703
Journal © 2019 Received 7 Aug 2019; revised 23 Sep 2019; accepted 23 Sep 2019; published 11 Oct 2019

Biomedical Optics EXPRESS

quantitatively measured with DRS by measurement of the reduced scattering coefficient, $\mu_s'(\lambda)$ [6,7].

DRS can be used to sense the morphological and biochemical changes that occur when normal colon tissue becomes pre-cancerous or cancerous [4,12,13], and thus, DRS has the potential to augment the performance of traditional WLE. However, the reliance of conventional DRS systems on optical fibers for reflectance collection limits system performance, limits scalability, and constrains the design options. In contrast, custom thin film silicon (Si) photodetectors (PDs) offer a high performance, scalable, and highly customizable alternative to optical fibers for reflectance collection in tissue DRS applications [14–18]. Si PDs improve performance over optical fibers since they have higher numerical apertures (NAs) and collect light from a larger fraction of the probe surface, they are highly scalable due to Si manufacturing technology, they can be geometrically optimized for specific applications, they can be implemented on a variety of substrates, including flexible or conformal, and they can be implemented in the instrument channel or as an attachment to an endoscope. Importantly, arrays of Si PDs can be used to perform spatially resolved DRS (SRDRS), which adds a spatial dimension to DRS by simultaneously measuring the tissue reflectance at multiple illumination-collection distances.

Previous reports on the development of a custom Si thin film multi-pixel endoscopic optical sensor (MEOS) leveraged the advantages of thin film Si PD based SRDRS systems for endoscopic applications such as colonoscopy [18]. A conceptual diagram of the system used to perform measurements with the MEOS is provided in Fig. 1. The MEOS consists of three concentric semi-annular 10 μm thick Si PDs bonded to a transparent glass substrate. The three Si PDs surround a shared 750 nm diameter illumination aperture, with at increasing mean radii of 450 μm, 540 μm, and 860 μm, for PDs 1, 2, and 3, respectively, and increasing PD widths of 58 μm, 100 μm, and 550 μm, respectively. The geometries of the custom PDs were optimized for measurement of colon tissue, and the MEOS was fabricated using standard Si microfabrication techniques [18]. The tissue (or tissue phantom) measured by the MEOS is interrogated by photons provided by an optical fiber coupled to the backside of the transparent glass substrate. Photons pass through the glass substrate and through the circular illumination aperture at the center of the three concentric PDs before sampling the tissue under measurement. Reflectance data is collected with the PDs in direct contact with the tissue and collected photons that have sampled the tissue are converted to electrical signals by the PDs [18].

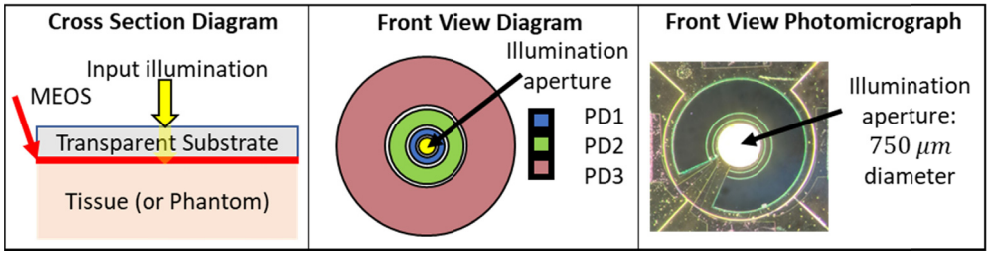

Fig. 1. Diagrams of MEOS cross section, front view diagram, and front view photomicrograph. In the cross-section diagram, red arrow points to the red layer representing the thin-film MEOS sensor.

Each of the three PDs in the MEOS system measure relative diffuse reflectance, as described by Eq. (1):

$$DR_{MEOS}(\lambda) = \frac{I_{meas}(\lambda)}{I_{ref}(\lambda)} \tag{1}$$

where $I_{meas}(\lambda)$ is the photocurrent generated by each PD due to light that has sampled the medium under measurement as a function of wavelength (λ), $I_{ref}(\lambda)$ is the photocurrent recorded

Biomedical Optics EXPRESS

during measurement of a reference phantom or reflectance standard, and both photocurrents have been calibrated to remove background current. Here, we report on the development of extraction of colon tissue optical properties (μ_s' and μ_a) from SRDRS measurements made using the prototype MEOS system, and demonstrate the extraction of tissue optical properties from MEOS measurements performed on normal and tumor ex-vivo human colon tissue.

2. Inverse model development and evaluation

2.1. Inverse model background

Methods to extract scattering and absorption from DRS spectra generally involve fitting a forward model to DRS measurements [6,7,19–24]. Forward models used for fitting include Monte Carlo (MC) [6], analytical models such as the diffusion approximation [23], and hybrid empirical-analytical models [24]. These approaches entail trade-offs between the computational time and the accuracy of the measured optical properties. Iterative fitting of forward MC models is highly accurate but slow, fitting of analytical models is fast but has undesirable inaccuracy [6], and empirically fit models can be highly accurate but require time consuming experimentation to calibrate each system [21]. Approaches have been taken to minimize the computational time of forward MC models [6], and to minimize the number of calibration measurements needed to implement an empirical model [25], but tradeoffs between accuracy, speed, and experimental overhead are still significant [22].

Another class of inverse models utilizes pre-calculated lookup tables (LUTs) of either MC modeled or experimentally measured reflectance [21,22]. If appropriate values of anisotropy (g) can be estimated for a tissue, and approximations of the spectral dependence of the dominant chromophores and scattering events can be assumed, LUTs offer the advantage of reduced computational time without compromising the accuracy of the modeling method.

Because the MEOS utilizes a multi-pixel PD, it is possible to develop two LUT extraction methods: one that computes the best LUT fit for each PD separately, and a second that computes the LUT fit for all three PDs simultaneously. In the following section these two extraction methods are developed, and then the extraction accuracy of the two methods is evaluated using experimentally measured MEOS data from eight validation tissue phantoms.

2.2. Description of LUT optical property extraction methods

Development and evaluation of MC populated LUT inverse models for the extraction of colon optical properties using the MEOS probe were based on the system in Fig. 1, using initial measured phantom and MC forward modeling studies previously reported [18].

The two methods of optical property extraction using LUT based inverse models evaluated herein are: (1) A spatially resolved LUT (SR-LUT), which extracts three pairs of optical properties (μ_s' and μ_a) at each measured wavelength (one pair for each of the three PDs); and (2) a new spatially constrained LUT (SC-LUT) method, enabled by the multi-pixel PDs, which extracts a single pair of optical properties for each measured wavelength. This SC-LUT method uses the reflectance from all three PDs simultaneously to extract μ_s' and μ_a, treating the sensed volume as homogeneous. Both methods are spectrally constrained by predefined μ_s' and μ_a wavelength-dependence, as described by Eq. (2) and Eq. (3).

For both methods, LUTs were generated for each PD by MC modeling reflectance for varied absorption and reduced scattering values. A total of 6000 MC simulations implemented in a graphics processing unit (GPU) enabled open-source MC light transport simulator [26,27] were performed to populate LUT reflectance for each of the three PDs with a uniform grid of 30 μ_s' levels and 200 μ_a levels. The light source was modeled as a cone with a divergence angle of 20° and a diameter of 750 μm at the illumination aperture. The refractive index for the modeled phantoms was 1.32 (water), and the refractive index of the detectors was 2.05 (due to the SiN

Biomedical Optics EXPRESS

coating on Si PDs). The reduced scattering coefficients (μ_s') ranged from 0.1 mm^{-1} to 3.1 mm^{-1}, and the absorption coefficients (μ_a) ranged from 0.00 mm^{-1} to 3.25 mm^{-1}, spanning the range of optical properties reported for colon tissue in the wavelength range from 450 nm to 750 nm [5,28–31]. All simulations were performed with the Henyey-Greenstein (HG) scattering phase function [32] and an anisotropy value of 0.92, which is close to the reported values of anisotropy for colon tissue for this wavelength range [33], and is also the average anisotropy of 1 μm polystyrene spheres in de-ionized (DI) water (polystyrene spheres were used to prepare liquid validation phantoms for extraction accuracy evaluation). The use of the HG rather than the Mie or another phase function was motivated by the availability of GPU-enhance MC modeling software [26,27], and was justified by previous work forward MC modeling the MEOS system using the HG phase function, where less than 10% MPE was achieved [18]. 2D interpolation was used to define diffuse reflectance surfaces $DR_{LUT}(\mu_s'(\lambda),\ \mu_a(\lambda))$ for μ_s' and μ_a values between and including the 6000 forward modeled pairs, using the MATLAB function *griddedInterpolant* [34]. Generation of the LUTs required approximately 20 minutes running on an Intel i7-8550U CPU with 16 GB of memory and an NVIDIA GeForce MX150 GPU. Comparison of forward modeling of phantom reflectance performed with a 3D as well as 2D simulation space indicated that a 2D model was justified, which permitted the propagation of a small number of photons per run (10^4). Figure 2 displays the reflectance surfaces for each of the three PDs. The MC modeled reflectance, which is computed as absolute reflectance, was scaled by a MC modeled reference medium with zero absorption to generate relative reflectance for comparison to experimental results. Likewise, experimental measurements of a single phantom prepared with the reference phantom optical properties were used to scale all experimental results.

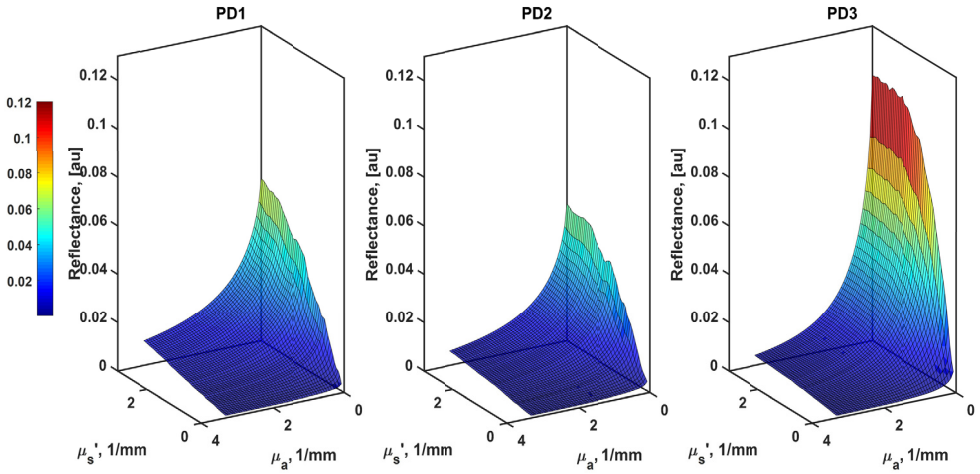

Fig. 2. Monte Carlo generated reflectance surfaces for the three PDs.

Measured reflectance spectra are fit to the LUT surfaces using nonlinear least squares minimization implemented with the *lsqnonlin* function in the MATLAB Optimization toolbox [35]. A commonly used approximation for $\mu_s'(\lambda)$ was adopted [19,36,37], as described by the following Eq. (2):

$$\mu_s'(\lambda) = A(\lambda)^{-B} \tag{2}$$

where A and B are coefficients that describe the power-law wavelength dependence of the reduced scattering coefficient. The absorption coefficient, $\mu_a(\lambda)$, was calculated using the wavelength dependent extinction coefficients of oxyhemoglobin and deoxyhemoglobin, $\in_{HbO2}(\lambda)$ and $\in_{Hb}(\lambda)$

Biomedical Optics EXPRESS

[38]:

$$\mu_a(\lambda) = C(D \in_{HbO2}(\lambda) + (1 - D)\in_{Hb}(\lambda)) \tag{3}$$

where C and D are the volume averaged total hemoglobin concentration and hemoglobin oxygen saturation, respectively [19,36,37]. Optical property extraction was achieved by fitting measured relative reflectance, $DR_{MEOS}(\lambda)$, to the LUT by finding values of A, B, C, and D which minimized the sum of squares difference between $DR_{LUT}(\mu_s'(\lambda),\ \mu_a(\lambda))$ and $DR_{MEOS}(\lambda)$, where $DR_{LUT}(\mu_s'(\lambda),\ \mu_a(\lambda))$ is the relative diffuse reflectance queried from the MC generated LUT at the values $\mu_s'(\lambda)$ and $\mu_a(\lambda)$. For the fitting process, the diffuse reflectance magnitude was scaled by the light-collecting surface area of each individual PD, A_{PD}.

For the SR-LUT method, the minimization occurs for each PD separately, and is described by Eq. (4):

$$\underset{A,\ B,\ C,D}{min}\ f(A,B,C,D) = \underset{A,\ B,\ C,D}{min} \sum\nolimits_{\lambda} ((DR_{LUT}(\mu_s'(\lambda),\ \mu_a(\lambda)) - DR_{MEOS}(\lambda))/A_{PD})^2 \tag{4}$$

where $f(A, B, C,\ D)$ defines the reduced scattering and absorption coefficients through Eqs. (1) and (2). Minimization using Eq. (4) results in extraction of $\mu_s'(\lambda)$, and $\mu_a(\lambda)$, for each of the three PDs independently, providing spatially resolved optical property extraction. In the case of measurements at N wavelengths, the dimension of the function being minimized is $N \times 1$.

Alternatively, for the SC-LUT method, all three of the PDs are evaluated simultaneously: the radial dependence of the reflectance is included in the modeling to increase the dimension of the minimization function to $N \times 3$. In this case, DR_{LUT}, and $DR_{MEOS}(\lambda)$ are $N \times 3$ matrices, A_{PD} is a vector of all three PD areas, and the minimization is described by Eq. (5):

$$\begin{aligned} &\underset{A,\ B,\ C,D}{min}\ f(A,B,C,D) \\ &\quad = \underset{A,\ B,\ C,D}{min} \sum\nolimits_{PD} \sum\nolimits_{\lambda} ((DR_{LUT}(\mu_s'(\lambda),\ \mu_a(\lambda), PD) - DR_{MEOS}(\lambda,\ PD))/A_{PD})^2 \end{aligned} \tag{5}$$

where the minimization across the three PDs is included by the term $\sum_{PD}$. A result of using the SC-LUT method of Eq. (5) is that the extracted optical properties are volume averaged over the entire sensed volume.

2.3. Experimental evaluation of the inverse method of optical property extraction

To evaluate the performance of the SR-LUT and SC-LUT for optical property extraction, eight liquid phantoms for validation were prepared with 1 μm diameter polystyrene spheres (Polysciences, Inc.) as the scattering agent, powdered hemoglobin (Sigma-Aldrich Co. LLC.) as the absorbing agent, and deionized (DI) water as the solvent. Optical absorption coefficients for the phantoms were calculated by measuring the absorption coefficient for concentrations of hemoglobin powder dissolved in DI water by a spectrophotometer (Shimadzu UV-3600) and calculating the extinction coefficient for the purchased hemoglobin chromophore. Based on the spectrophotometer resolution of measured extinction coefficients and precision of the microbalance used to prepare phantom solutions, the error in the theoretical value of μ_a was estimated to be approximately 1%. Reduced scattering coefficients for the solutions were calculated using an open-source program for calculating scattering from Mie theory [39]. The optical properties of the eight validation phantoms, as well as the reference phantom used for scaling in the wavelength range 450–750 nm at 10 nm wavelength intervals are shown in Fig. 3. The accuracy of the theoretical values of μ_s' calculated by Mie theory was primarily limited by the 3% coefficient of variance for the polystyrene scatterers [40]. The values of $\mu_s'(\lambda)$ shown in Fig. 3 and calculated by Mie theory for 1 μm diameter polystyrene spheres can be fit by Eq. (2) with 1.1% root-mean-square error, averaged across the 31 wavelengths used for validation.

Biomedical Optics EXPRESS

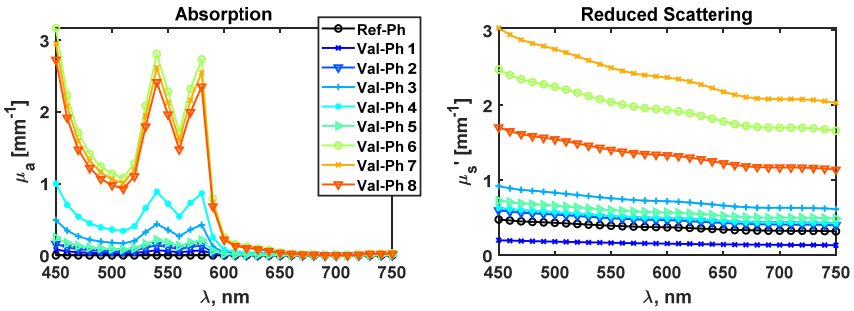

Fig. 3. The optical properties of the eight validation phantoms, as well as the reference phantom used for scaling, in the wavelength range 450 nm to 750 nm at 10 nm wavelength intervals.

Phantoms were measured with the probe surface placed into the liquid phantom solution such that the entire front face of each PD in the array was immersed. Illumination for all DRS measurements was provided by a 1 mm diameter optical fiber with a 0.39 NA (Thorlabs FT1000UMT). A 300 W Xenon lamp coupled to a Newport CS130 monochromator (TLS-300XU, Newport Corp.) provided the optical input to the 1 mm fiber and thus, to the MEOS probe. The PD photocurrents were measured using transimpedance amplifier (TIA) arrays. The TIA system used Texas Instruments TI IVC102 TIA chips for current integration, Adafruit ADS1015 chips for analog-to-digital conversion, and an Arduino Mega 2560 microcontroller to control integration times and data acquisition. All measurements with the TIA system were performed with a 100 ms integration time. For the phantom measurements performed between 450 nm and 750 nm, 4 minutes was required to acquire data at these 31 wavelengths. The TIA system and the monochromator were controlled using LabView. Repeated measurements of the same phantom without removing the MEOS device did not alter the measured reflectance more than 1% on average, thus settling of the phantoms was not considered to be a problem.

The performance of each of the two LUT inverse models described herein was quantified by the mean absolute value percent error between the values of $\mu_s'(\lambda)$ and $\mu_a(\lambda)$ calculated for each phantom based on their concentrations of hemoglobin and polystyrene spheres, and the corresponding values extracted from the measured reflectance using the SR-LUT and SC-LUT inverse models. The values of $\mu_s'(\lambda)$ and $\mu_a(\lambda)$ calculated from the phantom hemoglobin and polystyrene spheres are referred to herein as the theoretical values. Comparisons of the extracted verses theoretical values of the optical properties of the eight liquid phantoms for the two LUT extraction methods are displayed in Figs. 4 and 5 for the reduced scattering coefficients and the absorption coefficients, respectively. Figures 4 and 5 each display the average absolute value mean percent error (MPE) between the theoretical and extracted values for each phantom, as well as the overall average absolute value percent error across all eight phantoms.

For $\mu_s'(\lambda)$, the overall average error (averaged across all wavelengths and all three PDs) decreased from 13.25% to 6.38% going from the SR-LUT model to the SC-LUT model, and for $\mu_a(\lambda)$ the overall average error decreased from 31.42% to 8.38%. The time required to extract $\mu_s'(\lambda)$ and $\mu_a(\lambda)$ for each phantom was about 10 seconds for either the SR-LUT or the SC-LUT, but the extraction algorithm was not optimized for extraction speed. The MPE on for each of the three PDs for the SR-LUT model for μ_s' is 12.9%, 7.0%, and 19.9% for PDs 1, 2, and 3, respectively. For μ_a, the MPE is 16.5%, 11.9%, and 65.9% for PDs 1, 2, and 3, respectively. While the error for μ_a on PD 3 is higher than the error on the other two PDs, and the error on μ_s' for PD3 is higher than for the other PDs, differences in error on PD1 and PD2 are less pronounced. The difference may be due to lower signal magnitudes incident on PD3, which is furthest from the illumination source for low albedo phantoms. Additionally, some

Biomedical Optics EXPRESS

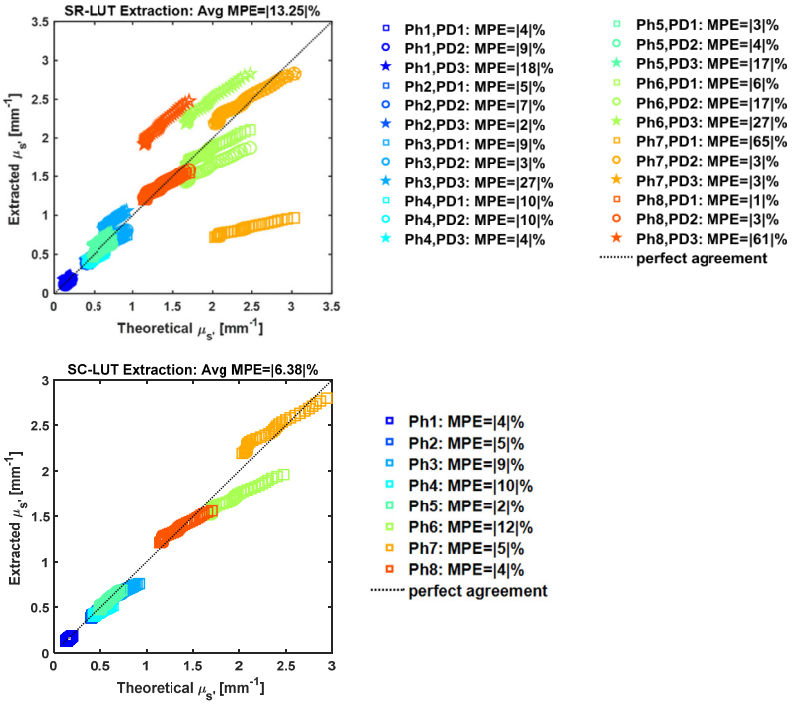

Fig. 4. Theoretical vs extracted reduced scattering coefficients for the six validation phantoms are shown for the SR-LUT (top) and SC-LUT (bottom). Theoretical coefficients are treated as true for error calculations.

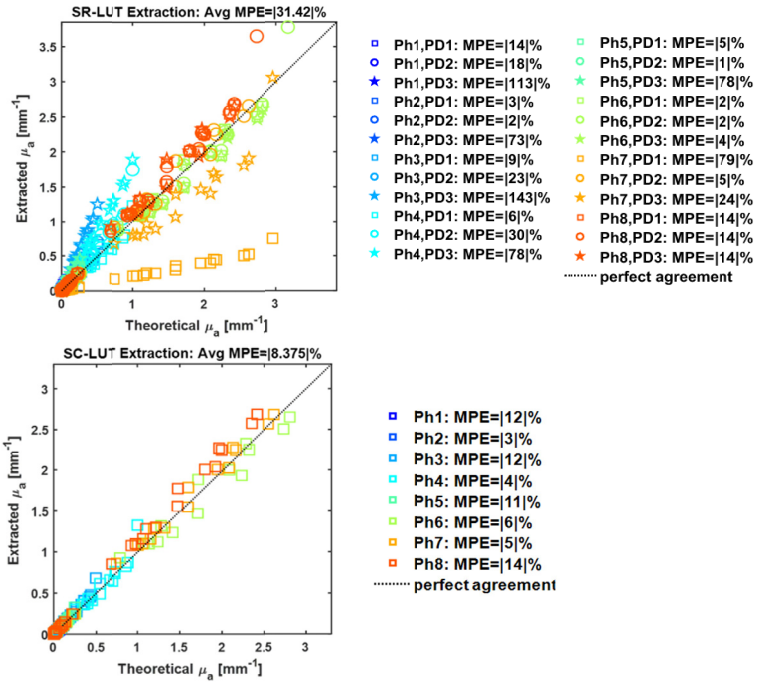

Fig. 5. Theoretical vs extracted absorption coefficients for the six validation phantoms are shown for the SR-LUT (top) and SC-LUT (bottom). Theoretical coefficients are treated as true for error calculations.

Biomedical Optics EXPRESS

amount of variation of reflectance agreement with modeling results could arise from sub-diffuse reflectance components. Researchers [41,42] have recently indicated that at short radial distances, higher order moments of the photon scattering phase-function may influence reflectance by as much as 10% [41], suggesting that in order to achieve the lowest possible discrepancy between experimental measurements and modeling, a higher order function than the Henyey-Greenstein phase function may be more desirable, and should be investigated in future studies of the MEOS system. Additionally, while prior researchers [6,43,44] have demonstrated that μ_s' may be used to accurately characterize scattering well beyond the 'diffusion approximation' [45], future work should investigate whether higher dimension LUTs could be implemented to improve extraction accuracy by accounting for sub-diffuse effects. However, for the purposes of achieving sufficient agreement between modeled and experimental reflectance for our system (<10% MPE) to enable comparison of optical property extraction methods, we believe that the Henyey-Greenstein phase function employed in this work is valid [18].

A clear improvement in extraction accuracy is achieved by extracting reduced scattering and absorption coefficients with the SC-LUT method compared to the SR-LUT method. This result is consistent with the findings of Tseng et al. [19], who found a similar improvement in optical property extraction accuracy by using both the spatial and spectral components of the diffuse reflectance collected by a fiber-based system, although the inverse model of Tseng et al. was based on iterative MC simulation rather than on LUTs. Using all three PDs together decreases the average extraction error to less than any individual PD would be able to achieve alone, as summarized by Table 1. A disadvantage of the SC-LUT method is that the output data loses possible depth information for each individual wavelength, since the tissue volume sampled by all three PDs is different and larger than for any single PD. Thus, the extracted optical properties from the SC-LUT are averaged over a larger volume than the properties extracted by the SR-LUT. For application to layered tissue (e.g. colon), the volume-averaged nature of optical properties measured with DRS should always be considered when analyzing experimental results and is especially important when comparing measurements with a different resolution of volume-averaging. While averaging over a larger volume with the SC-LUT compared to the SR-LUT is disadvantageous because it reduces the volume resolution of each probe measurement, it may also be advantageous because by averaging tissue measurements over a larger area, volume inhomogeneities, such as blood vessels, may be less likely to distort the measurements. Distortion of DRS measurements by blood vessel packaging of hemoglobin has been a criticism of DRS as a tissue diagnostic tool [46].

Table 1. Summary of average extraction errors for each PD for the SR-LUT and SC-LUT methods.

	SR-LUT Error %			SC-LUT Error %
	PD1	PD2	PD3	
μ_a	16.5	11.9	65.9	8.4
μ_s'	12.9	7.0	19.9	6.4
avg	14.7	9.4	42.9	7.4

3. Demonstration of extraction from ex-vivo human colon tissue

3.1. Human tissue measurement experimental procedure

Measurements of human colon tissue have been conducted, and the preliminary results described herein. The procedure for the human tissue study was developed to collect MEOS measurement data from excised human colon specimens within 30 min after resection from patients undergoing colectomy, where the colon was expected to have locations of tumor as well as normal tissue. This approach facilitated measurements on normal and tumor human colon tissue in as near as possible

Biomedical Optics EXPRESS

a biological condition to in-vivo tissue, but with minimized patient risk. The primary aim of the study was to determine the ability of the MEOS to quantitatively characterize absorption and scattering characteristics of different types of human colon tissue. To enable evaluation of measured tissue spectra with known histology, MEOS measurement locations were co-registered to a surgical biopsy by triangulating each MEOS measurement location using three sutures, which enabled tissue sections to be taken at each location for histopathologic analysis.

For each wavelength measured at each location, the MEOS system recorded 30 consecutive TIA current readings with an integration time of 100 ms for each TIA measurement. For measurements on human tissue, reflectance at 24 total wavelengths from 450 nm to 680 nm were recorded, requiring 3 minutes total acquisition time. Tissue optical properties are sensitive to applied pressure due to changes in blood perfusion as well as cellular crowding [47,48]. To ensure that a consistent force was applied by the sensor to the tissue being measured, the approach of Nichols et al. [49] was followed, where a custom pressure sensitive stage was developed consisting of an aluminum plate resting on four 5 lbf load cells. Prior to and following each set of human tissue measurements, the MEOS was measured on a reflectance standard (puck).

3.2. Human tissue measurement results and discussion

Preliminary MEOS measurements were performed on a single excised human colon, including two measurements performed at a single normal tissue location, and two measurements performed at a single tumor location to assess repeatability. During these repeated measurements, the MEOS probe was removed from contact with the tissue between measurements at the same location. The average percent difference between repeated measurements was 7.7%. The DRS spectra from these four measurements are displayed in Fig. 6, with a separate subplot for each of the three PDs, and error bars representing the standard deviation of the reflectance at each wavelength. The optical absorption and reduced scattering coefficients, μ_a and μ_s', were extracted from the DRS data shown in Fig. 6 using the SC-LUT inverse method detailed in Section 2, using the same LUTs generated for evaluation of the two inverse methods.

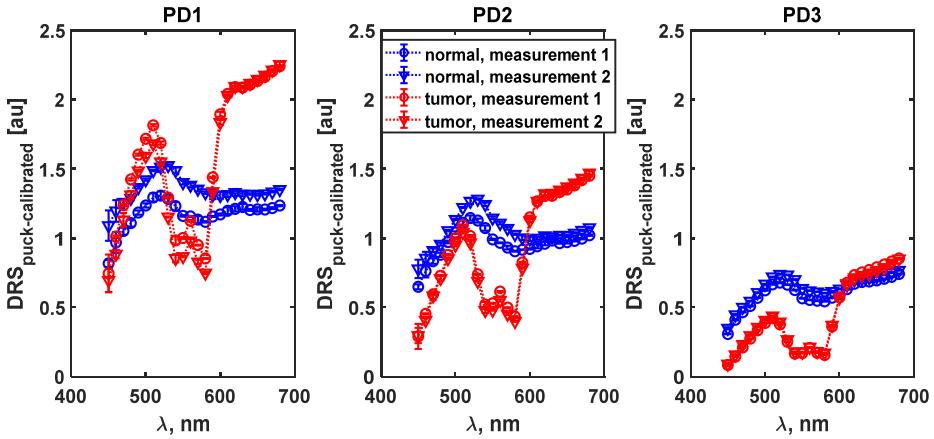

Fig. 6. DRS spectra measured with the MEOS prototype. Each subplot displays spectra with error bars obtained from two locations of excised colon (one normal and one tumor location), with two measurements performed at each location.

The values of μ_a and μ_s' extracted from these human colon tissue measurements are plotted in Fig. 7. Error bars on the data points plotted in Fig. 7 represent the average error observed at each wavelength for extraction of μ_a and μ_s' from the eight validation phantoms shown in Fig. 3. Although the optical properties plotted in Fig. 7 represent only a single site of each type

Biomedical Optics EXPRESS

of tissue for a single patient, they are still an interesting contribution to the literature because they were measured on ex-vivo tissue which was freshly excised and underwent minimal sample preparation (not frozen). The majority of reported optical properties for human colon tissue have been performed on tissue samples that have undergone freezing and thawing [5,29,30,50], which can significantly alter tissue optical properties [51].

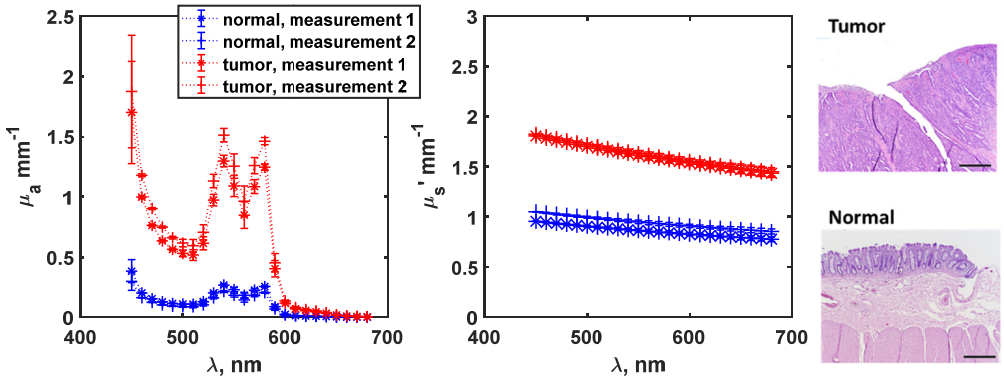

Fig. 7. Tissue absorption and reduced scattering coefficients extracted from the spectra provided in Fig. 7, with error bars, using the SC-LUT method. One the right, H&E-stained tissue sections of the two measured locations are displayed (both photomicrographs at 4x magnification, bar = 500 μm).

Values of μ_a and μ_s' for human colon tissue reported in the literature span a broad range. For example, at 500 nm, the value of μ_a for normal tissue ranges from 0.22 mm^{-1} [5] to 0.84 mm^{-1} [52], and for precancerous tissue from 0.37 mm^{-1} [31] to 0.60 mm^{-1} [5]. For μ_s', previously reported values for normal tissue range from 0.79 mm^{-1} [5,52] to 2.1 mm^{-1} [31], and for precancerous tissue from 0.55 mm^{-1} [5] to 2.36 mm^{-1} [31]. While the μ_a and μ_s' values for normal and tumor presented in Fig. 7 are not completely bracketed by previously reported values, the values are consistent given the large span of values reported. It is important to emphasize however, that the results presented here are representative for only one patient, and that the intention of including these results is to demonstrate the potential for applying the MEOS system to colon tissue optical property extraction, rather than validation of this technique's viability as a diagnostic tool.

4. Summary and conclusions

This paper describes and evaluates two inverse methods for extracting the reduced scattering and absorption coefficients, $\mu_s'(\lambda)$ and $\mu_a(\lambda)$, from reflectance measurements using the MEOS probe. Both extraction methods rely on lookup tables of Monte Carlo simulated diffuse reflectance. The first method, the SR-LUT method, extracts $\mu_s'(\lambda)$ and $\mu_a(\lambda)$ for each MEOS PD independently, yielding spatially resolved information. The second approach, the SC-LUT method, spatially constrains the extracted $\mu_s'(\lambda)$ and $\mu_a(\lambda)$ to the same values for each of the three MEOS PDs, yielding less error between the theoretical (true) and extracted absorption and reduced scattering coefficients. Eight liquid phantoms composed of polystyrene spheres and hemoglobin in deionized water were measured to experimentally evaluate the performance of these inverse methods on values of $\mu_s'(\lambda)$ and $\mu_a(\lambda)$ that spanned the range of reported values for colon in the 450–750 nm wavelength range. The SC-LUT was found to decrease the average extraction error of $\mu_s'(\lambda)$ and $\mu_a(\lambda)$ from 13.25% and 31.42%, respectively, to 6.38% and 8.38%, respectively. Additionally, preliminary measurements of ex-vivo human colon tissue were presented, and the optical properties μ_a and μ_s' were extracted from human tissue MEOS measurements that had

Biomedical Optics EXPRESS

less than 10% variation between repeated measurements. The MEOS multi-pixel custom Si PD probe extracts both spatial and spectral information with each measurement, and the use of the SC-LUT is able to leverage both spatial and spectral information together to yield lower tissue absorption and scattering coefficient extraction error compared to the use of the similar SR-LUT extraction method, which relies on spectral information alone.

Funding

Duke Cancer Institute (NIH CA014236).

Acknowledgements

The authors would like to thank Professor Martin A. Brooke, Associate Professor of Electrical and Computer Engineering (ECE), and Alyssa Lawrence, a former graduate student in ECE, both at Duke University, for the development of the TIA circuits used for MEOS photocurrent measurement. This work was supported by Duke University, in part through the MEDx program and the Duke Cancer Institute as part of the P30 Cancer Center Support Grant (Grant ID: NIH CA014236), and performed in part at the Duke University Shared Materials Instrumentation Facility (SMIF), a member of the North Carolina Research Triangle Nanotechnology Network (RTNN), which is supported by the National Science Foundation (Grant ECCS-1542015) as part of the National Nanotechnology Coordinated Infrastructure (NNCI). The authors would like to thank the staff of the Duke University SMIF for their technical assistance.

Disclosures

The authors declare that there are no conflicts of interest related to this article.

References

1. S. I. Bae and Y. S. Kim, "Colon cancer screening and surveillance in inflammatory bowel disease," Clin. Endosc. **47**(6), 509 (2014).
2. B. J. Qumseya, H. Wang, N. Badie, R. N. Uzomba, S. Parasa, D. L. White, H. Wolfsen, P. Sharma, and M. B. Wallace, "Advanced imaging technologies increase detection of dysplasia and neoplasia in patients with barrett's esophagus: A meta-analysis and systematic review," Clin. Gastroenterol. Hepatol. **11**(12), 1562–1570.e2 (2013).
3. M. Iacucci, T. Uraoka, M. Fort Gasia, and N. Yahagi, "Novel diagnostic and therapeutic techniques for surveillance of dysplasia in patients with inflammatory bowel disease," Can. J. Gastroenterol. Hepatol. **28**(7), 361–370 (2014).
4. A. Dhar, K. S. Johnson, M. R. Novelli, S. G. Bown, I. J. Bigio, L. B. Lovat, and S. L. Bloom, "Elastic scattering spectroscopy for the diagnosis of colonic lesions: Initial results of a novel optical biopsy technique," Gastrointest. Endosc. **63**(2), 257–261 (2006).
5. G. I. Zonios, R. M. Cothren, J. T. Arendt, J. Wu, J. VanDam, J. M. Crawford, R. Manoharan, and M. S. Feld, "Morphological model of human colon tissue fluorescence," Ieee Trans. Biomed. Eng. **43**(4), 437 (1996).
6. G. M. Palmer and N. Ramanujam, "Monte Carlo-based inverse model for calculating tissue optical properties. Part I: Theory and validation on synthetic phantoms," Appl. Opt. **45**(5), 1062–1071 (2006).
7. A. Kienle, L. Lilge, M. S. Patterson, R. Hibst, R. Steiner, and B. C. Wilson, "Spatially resolved absolute diffuse reflectance measurements for noninvasive determination of the optical scattering and absorption coefficients of biological tissue," Appl. Opt. **35**(13), 2304–2314 (1996).
8. S. Coda, P. D. Siersema, G. W. H. Stamp, A. V. Thillainayagam, E. I. Open, S. Coda, P. C. Road, and U. Kingdom, "Biophotonic endoscopy: a review of clinical research techniques for optical imaging and sensing of early gastrointestinal cancer," Endosc. Int. open **3**(5), E380–E392 (2015).
9. E. Rodriguez-Diaz, Q. Huang, S. R. Cerda, M. J. O'Brien, I. J. Bigio, and S. K. Singh, "Endoscopic histological assessment of colonic polyps by using elastic scattering spectroscopy," Gastrointest. Endosc. **81**(3), 539–547 (2015).
10. P. Thueler, I. Charvet, F. Bevilacqua, M. St Ghislain, G. Ory, P. Marquet, P. Meda, B. Vermeulen, and C. Depeursinge, "In vivo endoscopic tissue diagnostics based on spectroscopic absorption, scattering, and phase function properties," J. Biomed. Opt. **8**(3), 495 (2003).
11. I. J. Bigio and S. Fantini, *Quantitative Biomedical Optics: Theory, Methods, and Applications* (Cambridge University Press, 2016).
12. E. Rodriguez-Diaz, C. Atkinson, L. I. Jepeal, A. Berg, C. S. Huang, S. R. Cerda, M. J. O'Brien, I. J. Bigio, F. A. Farraye, and S. K. Singh, "Elastic scattering spectroscopy as an optical marker of inflammatory bowel disease activity and subtypes," Inflamm. Bowel Dis. **20**(6), 1029–1036 (2014).

Biomedical Optics EXPRESS

13. Z. Ge, K. T. Schomacker, and N. S. Nishioka, "Identification of colonic dysplasia and neoplasia by diffuse reflectance spectroscopy and pattern recognition techniques," Appl. Spectrosc. **52**(6), 833–839 (1998).
14. S. Dhar, J. Lo, B. Yu, M. A. Brooke, N. Ramanujam, and N. M. Jokerst, "Custom annular photodetector arrays for breast cancer margin assessment using diffuse reflectance spectroscopy," in *Biomedical Circuits and Systems Conference (BioCAS), 2011 IEEE* (IEEE, 2011), pp. 440–443.
15. S. Dhar, D. M. Miller, and N. M. Jokerst, "High responsivity, low dark current, heterogeneously integrated thin film Si photodetectors on rigid and flexible substrates," Opt. Express **22**(5), 5052–5059 (2014).
16. O. Senlik and N. M. Jokerst, "Concentric Multi-Pixel Silicon Photodiode Array Probes for Spatially Resolved Diffuse Reflectance Spectroscopy," IEEE J. Sel. Top. Quantum Electron. **22**(3), 4–5 (2016).
17. D. M. Miller and N. M. Jokerst, "Flexible silicon sensors for diffuse reflectance spectroscopy of tissue," Biomed. Opt. Express **8**(3), 1512–1524 (2017).
18. B. Lariviere, K. S. Garman, N. L. Ferguson, D. A. Fisher, and N. M. Jokerst, "Spatially resolved diffuse reflectance spectroscopy endoscopic sensing with custom Si photodetectors," Biomed. Opt. Express **9**(3), 1164–1176 (2018).
19. T.-Y. Tseng, C.-Y. Chen, Y.-S. Li, and K.-B. Sung, "Quantification of the optical properties of two-layered turbid media by simultaneously analyzing the spectral and spatial information of steady-state diffuse reflectance spectroscopy," Biomed. Opt. Express **2**(4), 901–914 (2011).
20. T. J. Farrell, B. C. Wilson, and M. S. Patterson, "The use of a neural network to determine tissue optical properties from spatially resolved diffuse reflectance measurements," Phys. Med. Biol. **37**(12), 2281–2286 (1992).
21. N. Rajaram, T. Nguyen, and J. W. Tunnell, "Lookup table–based inverse model for determining optical properties of turbid media," J. Biomed. Opt. **13**(5), 050501 (2008).
22. R. J. Hennessy, S. L. Lim, M. K. Markey, and J. W. Tunnell, "Monte Carlo lookup table-based inverse model for extracting optical properties from tissue-simulating phantoms using diffuse reflectance spectroscopy," J. Biomed. Opt. **18**(3), 037003 (2013).
23. T. J. Farrell, M. S. Patterson, and B. Wilson, "A diffusion theory model of spatially resolved, steady-state diffuse reflectance for the noninvasive determination of tissue optical properties in vivo," Med. Phys. **19**(4), 879–888 (1992).
24. R. Reif, O. A'Amar, and I. J. Bigio, "Analytical model of light reflectance for extraction of the optical properties in small volumes of turbid media," Appl. Opt. **46**(29), 7317–7328 (2007).
25. B. S. Nichols, N. Rajaram, J. W. Tunnell, B. S. Nichols, N. Rajaram, and J. W. Tunnell, "Performance of a lookup table-based approach for measuring tissue optical properties with diffuse optical spectroscopy," J. Biomed. Opt. **17**(5), 057001 (2012).
26. Q. Fang and D. A. Boas, "Monte Carlo simulation of photon migration in 3D turbid media accelerated by graphics processing units," Opt. Express **17**(22), 20178–20190 (2009).
27. L. Yu, F. Nina-Paravecino, D. R. Kaeli, and Q. Fang, "Scalable and massively parallel Monte Carlo photon transport simulations for heterogeneous computing platforms," J. Biomed. Opt. **23**(1), 010504 (2018).
28. H. Ao, D. Xing, H. Wei, H. Gu, G. Wu, and J. Lu, "Thermal coagulation-induced changes of the optical properties of normal and adenomatous human colon tissues in vitro in the spectral range 400-1,100 nm," Phys. Med. Biol. **53**(8), 2197–2206 (2008).
29. H. Wei, D. Xing, G. Wu, H. Gu, J. Lu, Y. Jin, and X.-Y. Li, "Differences in optical properties between healthy and pathological human colon tissues using a Ti:sapphire laser: an *in vitro* study using the Monte Carlo inversion technique," J. Biomed. Opt. **10**(4), 044022 (2005).
30. H.-J. Wei, D. Xing, J.-J. Lu, H.-M. Gu, G.-Y. Wu, and Y. Jin, "Determination of optical properties of normal and adenomatous human colon tissues in vitro using integrating sphere techniques," World J. Gastroenterol. **11**(16), 2413–2419 (2005).
31. S. Carvalho, N. Gueiral, E. Nogueira, R. Henrique, L. Oliveira, and V. V. Tuchin, "Comparative study of the optical properties of colon mucosa and colon precancerous polyps between 400 and 1000 nm," Proc. SPIE **10063**, 100631L (2017).
32. S. A. Prahl, "A Monte Carlo model of light propagation in tissue," in *Dosimetry of Laser Radiation in Medicine and Biology* (International Society for Optics and Photonics, 1989), Vol. 10305, p. 1030509.
33. S. L. Jacques, "Optical properties of biological tissues: a review," Phys. Med. Biol. **58**(11), R37–R61 (2013).
34. "MATLAB griddedInterpolant," (2018).
35. "MATLAB lsqnonlin," (2018).
36. R. M. Doornbos, R. Lang, M. C. Aalders, F. W. Cross, and H. J. Sterenborg, "The determination of in vivo human tissue optical properties and absolute chromophore concentrations using spatially resolved steady-state diffuse reflectance spectroscopy," Phys. Med. Biol. **44**(4), 967–981 (1999).
37. P. R. Bargo, S. A. Prahl, T. T. Goodell, R. A. Sleven, G. Koval, G. Blair, and S. L. Jacques, "In vivo determination of optical properties of normal and tumor tissue with white light reflectance and an empirical light transport model during endoscopy," J. Biomed. Opt. **10**(3), 034018 (2005).
38. S. Prahl, "Hemoglobin Spectra," https://omlc.org/spectra/hemoglobin/summary.html.
39. Maetzler, "Maetzler's MATLAB code for Mie theory," https://omlc.org/software/mie/.
40. "Polysciences 1 micron spheres datasheet," https://www.polysciences.com/default/catalog-products/microspheres-particles/polymer-microspheres/polybead-sup-r-sup-microspheres/polybead-sup-r-sup-non-functionalized-microspheres/polybead-microspheres-100181m/.

Biomedical Optics EXPRESS

41. P. Naglic, F. Pernuš, B. Likar, and M. Bürmen, "Estimation of optical properties by spatially resolved reflectance spectroscopy in the subdiffusive regime," J. Biomed. Opt. **21**(9), 095003 (2016).
42. J. J. Bravo, K. D. Paulsen, D. W. Roberts, and S. C. Kanick, "Sub-diffuse optical biomarkers characterize localized microstructure and function of cortex and malignant tumor," Opt. Lett. **41**(4), 781–784 (2016).
43. A. Kienle and M. S. Patterson, "Determination of the optical properties of turbid media from a single Monte Carlo simulation," Phys. Med. Biol. **41**(10), 2221–2227 (1996).
44. R. Graaff, M. H. Koelink, F. F. M. De Mul, W. G. Zijlstra, A. C. M. Dassel, and J. G. Aarnoudse, "Condensed Monte Carlo simulations for the description of light transport," Appl. Opt. **32**(4), 426–434 (1993).
45. G. Zonios, L. T. Perelman, V. Backman, R. Manoharan, M. Fitzmaurice, J. Van Dam, and M. S. Feld, "Diffuse reflectance spectroscopy of human adenomatous colon polyps in vivo," Appl. Opt. **38**(31), 6628–6637 (1999).
46. C. Lau, O. R. Scepanovic, J. Mirkovic, S. McGee, C.-C. Yu, S. F. Fulghum, M. B. Wallace, J. W. Tunnell, K. L. Bechtel, and M. S. Feld, "Re-evaluation of model-based light-scattering spectroscopy for tissue spectroscopy," J. Biomed. Opt. **14**(2), 024031 (2009).
47. B. Yu, A. Shah, V. K. Nagarajan, and D. G. Ferris, "Diffuse reflectance spectroscopy of epithelial tissue with a smart fiber-optic probe," Biomed. Opt. Express **5**(3), 675 (2014).
48. B. S. Nichols, C. E. Schindler, J. Q. Brown, L. G. Wilke, C. S. Mulvey, M. S. Krieger, J. Gallagher, J. Geradts, R. A. Greenup, J. A. Von Windheim, and N. Ramanujam, "A Quantitative Diffuse Reflectance Imaging (QDRI) system for comprehensive surveillance of the morphological landscape in breast tumor margins," PLoS One **10**(6), e0127525 (2015).
49. B. S. Nichols, A. Llopis, G. M. Palmer, S. S. McCachren, O. Senlik, D. Miller, M. A. Brooke, N. M. Jokerst, J. Geradts, and R. Greenup, "Miniature spectral imaging device for wide-field quantitative functional imaging of the morphological landscape of breast tumor margins," J. Biomed. Opt. **22**(2), 026007 (2017).
50. H. Ao, D. Xing, H. Wei, H. Gu, G. Wu, and J. Lu, "Thermal coagulation-induced changes of the optical properties of normal and adenomatous human colon tissues in vitro in the spectral range 400–1100 nm," Phys. Med. Biol. **53**(8), 2197–2206 (2008).
51. G. M. Palmer, C. L. Marshek, K. M. Vrotsos, and N. Ramanujam, "Optimal methods for fluorescence and diffuse reflectance measurements of tissue biopsy samples," Lasers Surg. Med. **30**(3), 191–200 (2002).
52. R. Marchesini, E. Pignoli, and S. Tomatis, "Ex Vivo Optical Properties of Human Colon Tissue," Lasers Surg. Med. **15**(4), 351–357 (1994).